SUPPLEMENTAL INFORMATION

Neuromedin S-Producing Neurons Act as Essential Pacemakers in the Suprachiasmatic Nucleus to Couple Clock Neurons and Dictate Circadian Rhythms

Ivan T. Lee,[1,2,5] Alexander S. Chang,[1,5] Manabu Manandhar,[1,5] Yongli Shan,[2] Junmei Fan,[2] Mariko Izumo,[2] Yuichi Ikeda,[1,3] Toshiyuki Motoike,[1,2,3] Shelley Dixon,[1,2,3] Jeffrey E. Seinfeld,[2] Joseph S. Takahashi,[2,3,4,*] Masashi Yanagisawa[1,3,4,*]

[1]Department of Molecular Genetics

[2]Department of Neuroscience

[3]Howard Hughes Medical Institute

University of Texas Southwestern Medical Center, 5323 Harry Hines Blvd., Dallas, TX 75390, USA

[4]International Institute for Integrative Sleep Medicine (WPI-IIIS), University of Tsukuba, Tsukuba 305-8575, Japan

[5]These authors contributed equally to this work

*Equal corresponding authors: joseph.takahashi@utsouthwestern.edu, masashi.yanagisawa@utsouthwestern.edu

Supplemental Figure Legends

Figure S1, related to Figure 1. *Nms* Expression in C57BL/6J Mouse Brain

(A) Representative brain slices from C57BL/6J mice hybridized to anti-sense ^{35}S-labeled *Nms* riboprobe. The SCN is encircled in red. Only the forebrain was examined.

(B) Higher (dark field) magnification of SCN sections.

Figure S2, related to Figure 1. Schematic of Mating Crosses

(A) Several generations of crosses were used to produce the *tetO* transgene-containing mice presented in this paper. Mice shaded in light gray represent mice that were used for subsequent crosses. The mouse shaded in dark gray represents the key experimental mouse genotype.

(B) Crosses used to produce the experimental mouse genotypes that contain both the *tetO* transgene and the PER2::LUC transgene. The connotation of the shading is similar to (A).

Figure S3, related to Figure 1. HA (*Nms*) Expression in the *Nms-Clock*$^{\Delta 19}$ Mouse Brain

Representative brain slices from *Nms-Clock*$^{\Delta 19}$ mice are stained with anti-HA. Panels are organized relatively from anterior to posterior. Outside of the SCN, staining can be observed in the Edinger-Westphal nucleus, dorsomedial hypothalamic nucleus, anterior hypothalamic area, ventromedial thalamic nucleus, lateroanterior hypothalamic nucleus, posterior hypothalamic nucleus, median preoptic nucleus, retromammillary nucleus, retrochiasmatic area, external cortex of the inferior colliculus, and pyramidal tract. Not all staining are visibly displayed here.

Abbreviations (for Figure S3 and S7) using nomenclature from Franklin and Paxinos (2008): DEn, dorsal endopiriform claustrum; IEn, intermediate endopiriform claustrum; AOL, anterior olfactory area, lateral part; AOM, anterior olfactory area, medial part; AOP, anterior olfactory area posterior part; DTT, dorsal tenia tecta; VO,ventral orbital cortex; LO, lateral orbital cortex;

aci, anterior commissure, intrabulbar part; CPu, caudate putamen (striatum); aca, anterior commissure, anterior part; AcbC, accumbens nucleus, core; LSI, lateral septal nucleus, intermediate part; MS, medial septal nucleus; MnPO, median preoptic nucleus; LPO, lateral preoptic area; +MPOM, medial preoptic nucleus, medial part; MPOL, medial preoptic nucleus, lateral part; MPA, medial preoptic area; AVPe, anteroventral periventricular nucleus; VLPO, ventrolateral preoptic nucleus; PVA, paraventricular thalamic nucleus, anterior part; AM, anteromedial thalamic nucleus; CM, central medial thalamic nucleus; Re, reuniens thalamic nucleus; Rh, rhomboid thalamic nucleus; VL, ventrolateral thalamic nucleus; VM, ventromedial thalamic nucleus; PLH, peduncular part of lateral hypothalamus; AHA, anterior hypothalamic area, anterior part; LA, lateroanterior hypothalamic nucleus; SCN, suprachiasmatic nucleus; VA, Ventral anterior thalamic nucleus; BMA, basomedial amygdaloid nucleus, anterior part; ACo, anterior cortical amygdaloid area; MeAD, medial amygdaloid nucleus, anterodorsal part; MeAV, medial amygdaloid nucleus, anteroventral part; AHP, anterior hypothalamic area, posterior part; AHC, anterior hypothalamic area, central part; TuLH, tuberal region of lateral hypothalamus; VMH, ventromedial hypothalamic nucleus; RSD, retrosplenial dysgranular cortex; RSGc, retrosplenial granular cortex c region; MPtA, medial parietal association cortex; DM, dorsomedial hypothalamic nucleus; VMHDM, ventromedial hypothalamic nucleus, dorsomedial part; VMHVL, ventromedial hypothalamic nucleus, ventrolateral part; Arc, arcuate hypothalamic nucleus; MePD, medial amygdaloid nucleus, posterodorsal part; MePV, medial amygdaloid nucleus, posteroventral part; cp, cerebral peduncle; VPL, ventral posterolateral thalamic nucleus; VPM, ventral posteromedial thalamic nucleus; ZID, zona incerta, dorsal part; ZIV, zona incerta,ventral part; CA1, field CA1 of the hippocampus; CA3, field CA3 of the hippocampus; DG, dentate gyrus; DLG, dorsal lateral geniculate nucleus; PGPC, pregeniculate nucleus,

parvicellular part; PGMC, pregeniculate nucleus, magnocellular part; Po, posterior thalamic nuclear group; PH, posterior hypothalamic nucleus; PAG, periaqueductal gray; APTD, anterior pretectal nucleus, dorsal part; PCom, nucleus of the posterior commissure; MCPC, magnocellular nucleus of the posterior commissure; InWh, intermediate white layer of the superior colliculus; InG, intermediate gray layer of the superior colliculus, Op, optic nerve layer of the superior colliculus; Dk, nucleus of Darkschewitsch; EW, Edinger-Westphal nucleus; MGD, medial geniculate nucleus, dorsal part; MGV, medial geniculate nucleus, ventral part; SNR, substantia nigra, reticular part; VTA, ventral tegmental area; MM, medial mammillary nucleus, medial part; ML, medial mammillary nucleus, lateral part; RM, retoromammillary nucleus; AHiPM, amygdalohippocampal area, posteromedial part; PMCo, posteromedial cortical amygdaloid area; BLP, basolateral amygdaloid nucleus, posterior part; SuVe, superior vestibular nucleus; LC, locus coeruleus; LDTg, laterodorsal tegmental nucleus; DTgP, dorsal tegmental nucleus, pericentral part; IRt, intermediate reticular nucleus; DMTg, dorsomedial tegmental area; MVeMC, medial vestibular nucleus, magnocellular part; MVePC medial vestibular nucleus, parvicellular part; Pr, prepositus nucleus; Gi, gigantocellular reticular nucleus; RMg, raphe magnus nucleus; py, pyramidal tract; ml, medial lemniscus; VeCb, vestibulocerebellar nucleus; 4/5Cb, lobules 4 and 5 of the cerebellar vermis; icp, inferior cerebellar peduncle.

Figure S4, related to Figure 1. Distribution of VIP and GRP-Expressing Neurons in the Mouse SCN

(A) Double staining of GRP (green) and VIP (red) on SCN sections of colchicine-treated C57BL/6J mice. TO-PRO-3 counterstains the nuclei. The scale bar is 50 μm. Quantitative data are shown to the right.

Figure S5, related to Figure 2. *Clock*$^{\Delta 19}$ Expression within VIP-Producing Neurons in the SCN Does Not Lengthen Behavioral Circadian Period

(A and B) Double staining of HA (green) and VIP (red) on SCN sections of *Vip-Clock*$^{\Delta 19}$ mice. TO-PRO-3 counterstains the nuclei. Scale bars are 50 μm in (A) and 5 μm in (B). Quantitative data are shown at the bottom in (B).

(C) Double staining of HA (green) and AVP (red) on SCN sections of *Vip-Clock*$^{\Delta 19}$ mice. Scale bars are 50 μm. HA-positive cells do not co-localize with AVP-immunoreactive neurons.

(D) Representative actograms of *Vip-Clock*$^{\Delta 19}$ (bottom panel) and *R26-Vip* (top panel) mice. Colored bars represent the days of analyses presented in (E).

(E) Quantification of circadian activity in *Vip-Clock*$^{\Delta 19}$ transgenic and *R26-Vip* control mice. Mean free-running period, amplitude, and average activity counts were not significantly different between the genotypes (Student's t-test, $p>0.05$; *R26-Vip*, n=9; *Vip-Clock*$^{\Delta 19}$, n=9). Values are presented as mean ± SEM.

Figure S6, related to Figure 3. NMS and YFP co-localization in *Nms-iCre;YFP* SCN, and loss of synchrony in *Nms-Bmal1*$^{fl/fl}$ mice.

(A) Double staining of YFP (green) and NMS (red) on SCN sections of *Nms-iCre;YFP* mice using anti-GFP and anti-NMS antibodies, respectively. The scale bars are 50 μm (top panels) and 5 μm (bottom panels). Quantitative data are shown to the right.

(B) Representative raster and Rayleigh plots of PER2::LUC oscillation in 50 individual neurons from the SCN of adult *Bmal1*$^{fl/fl}$ and *Nms-Bmal1*$^{fl/fl}$ mice. In the raster plot, the red corresponds to peak bioluminescence and the green to trough. The length of the arrow in the Rayleigh plot represents the strength of synchronization.

Figure S7, related to Figure 6. Distribution of GFP (*Nms)*-Expressing Neurons in the Mouse Brain

Representative brain slices from *Nms-TeNT* mice were stained with anti-GFP. Panels are organized relatively from anterior to posterior. Outside of the SCN, staining can be observed in the Edinger-Westphal nucleus, dorsomedial hypothalamic nucleus, lateroanterior hypothalamic nucleus, posterior hypothalamic nucleus, median preoptic nucleus, medial preoptic nucleus, and retromammillary nucleus. Not all regions with staining are displayed here. Names of the abbreviations are listed in Figure S2.

Table S1, related to Figures 1-7. List of Mouse Lines.

Abbreviations	Full Description of Genotypes	Phenotype
R26	*ROSA-STOP-tTA$^{KI/KI}$*	Normal rhythms
R26-Nms	*Nms-iCre; ROSA-STOP-tTA$^{KI/KI}$*	Normal rhythms
R26-Clock$^{\Delta 19}$	*ROSA-STOP-tTA$^{KI/KI}$; tetO-Clock$^{\Delta 19}$*	Normal rhythms
Nms-Clock$^{\Delta 19}$	*Nms-iCre; ROSA-STOP-tTA$^{KI/KI}$; tetO-Clock$^{\Delta 19}$*	Dox-reversible lengthening of period
R26-Nms;Luc	*Nms-iCre; ROSA-STOP-tTA$^{KI/KI}$; PER2$^{LUC/+}$*	Normal rhythms
R26-Clock$^{\Delta 19}$;Luc	*ROSA-STOP-tTA$^{KI/KI}$; tetO-Clock$^{\Delta 19}$; PER2$^{LUC/+}$*	Normal rhythms
Nms-Clock$^{\Delta 19}$;Luc	*Nms-iCre; ROSA-STOP-tTA$^{KI/KI}$; tetO-Clock$^{\Delta 19}$; PER2$^{LUC/+}$*	Lengthened period
R26-Vip	*Vip-Cre$^{KI/KI}$; ROSA-STOP-tTA$^{KI/KI}$*	Normal rhythms
Vip-Clock$^{\Delta 19}$	*Vip-Cre$^{KI/KI}$; ROSA-STOP-tTA$^{KI/KI}$; tetO-Clock$^{\Delta 19}$*	Normal rhythms
Nms-iCre;YFP	*Nms-iCre; ROSA-STOP-YFP$^{KI/KI}$*	*Nms* distribution replicated
Bmal1$^{fl/fl}$	*Bmal1$^{fl/fl}$*	Normal rhythms
Nms-Bmal1$^{fl/+}$	*Nms-iCre; Bmal1$^{fl/+}$*	Normal rhythms
Nms-Bmal1$^{fl/fl}$	*Nms-iCre; Bmal1$^{fl/fl}$*	Loss of rhythms
Nms-Bmal1$^{fl/fl}$;YFP	*Nms-iCre; Bmal1$^{fl/fl}$; ROSA-STOP-YFP$^{KI/KI}$*	*Bmal1* deletion in *Nms* cells assessed
Nms-Bmal1$^{fl/fl}$;Luc	*Nms-iCre; Bmal1$^{fl/fl}$; PER2$^{LUC/LUC}$*	Desynchronized
R26-Per2	*ROSA-STOP-tTA$^{KI/KI}$; tetO-Per2*	Normal rhythms
Nms-Per2	*Nms-iCre; ROSA-STOP-tTA$^{KI/KI}$; tetO-Per2*	Dox-reversible loss of rhythms
R26-Per2;Luc	*ROSA-STOP-tTA$^{KI/KI}$; tetO-Per2; PER2$^{LUC/+}$*	Normal rhythms
Nms-Per2;Luc	*Nms-iCre; ROSA-STOP-tTA$^{KI/KI}$; tetO-Per2; PER2$^{LUC/+}$*	Damped/desynchronized
Nms-/-	*Nms-/-*	Normal rhythms
Nmu-/-	*Nmu-/-*	Normal rhythms

Nms$^{-/-}$*Nmu*$^{-/-}$	*Nms-/-; Nmu-/-*	Normal rhythms
R26-TeNT	*ROSA-STOP-tTA*$^{KI/KI}$*; tetO-TeNT*	Normal rhythms
Nms-TeNT	*Nms-iCre; ROSA-STOP-tTA*$^{KI/KI}$*; tetO-TeNT*	Dox-reversible loss of rhythms
R26-Nms;SynGFP	*Nms-iCre; ROSA-STOP-tTA*$^{KI/KI}$*; tetO-SynGFP*	VAMP2 cleavage control
Nms-TeNT;SynGFP	*Nms-iCre; ROSA-STOP-tTA*$^{KI/KI}$*; tetO-TeNT; tetO-SynGFP*	VAMP2 cleavage confirmed
R26-TeNT;Luc	*ROSA-STOP-tTA*$^{KI/KI}$*; tetO-TeNT; PER2*$^{LUC/+}$	Normal rhythms
Nms-TeNT;Luc	*Nms-iCre; ROSA-STOP-tTA*$^{KI/KI}$*; tetO-TeNT; PER2*$^{LUC/+}$	Damped/desynchronized
Note: Single tetO transgenic mouse lines previously published are not listed here.		

A

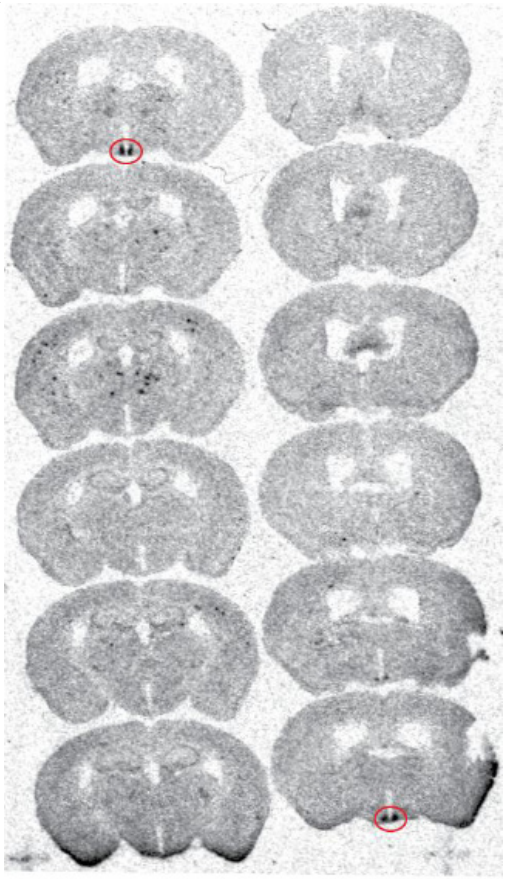

B

Nms sense

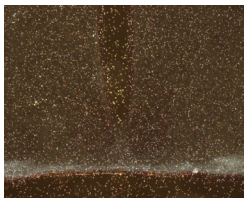

Nms anti-sense

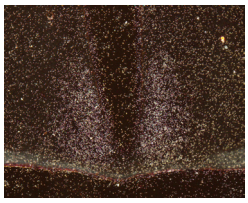

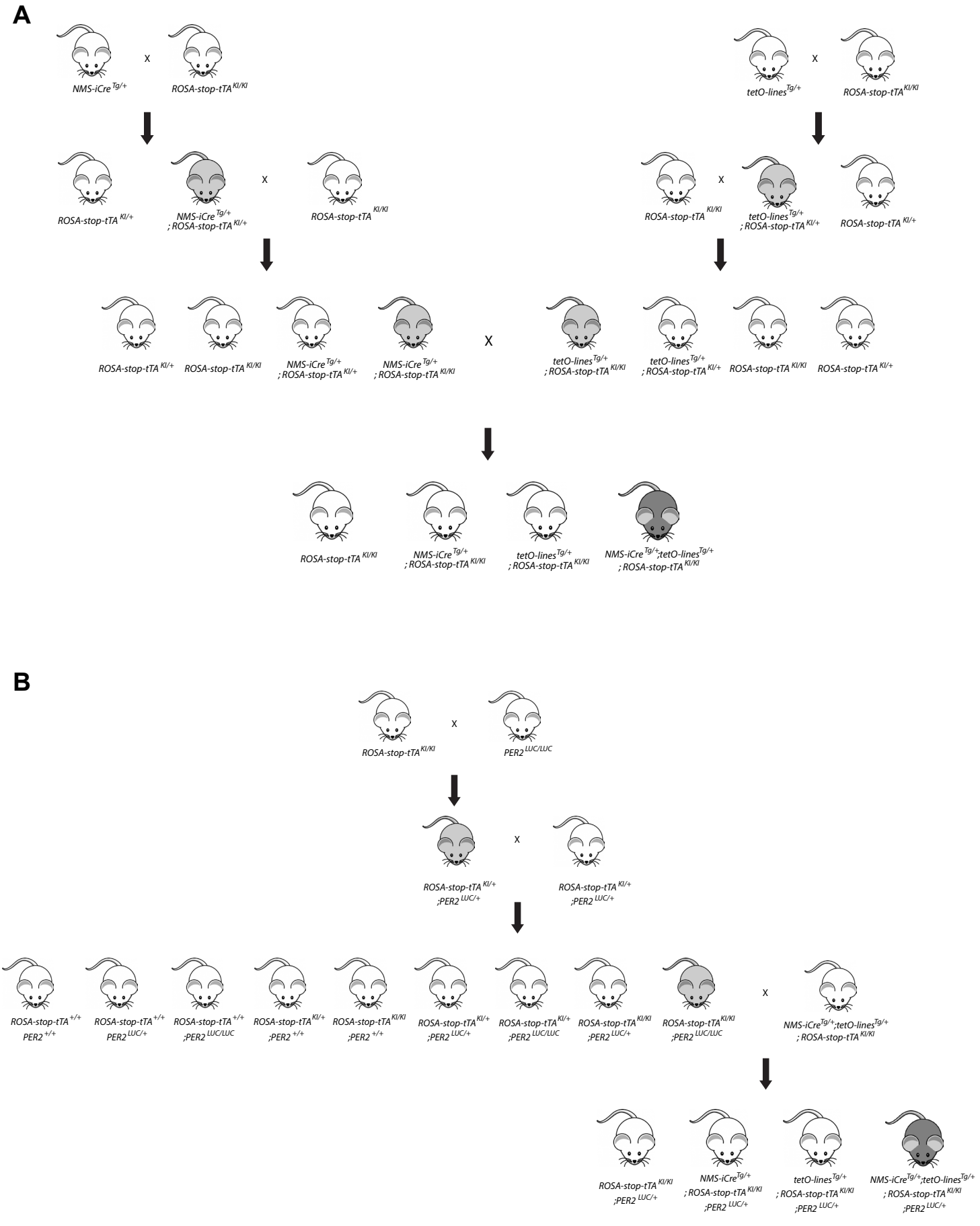
A
NMS-iCre Tg/+
x
ROSA-stop-tTA KI/KI
tetO-lines Tg/+
x
ROSA-stop-tTA KI/KI
ROSA-stop-tTA KI/+
NMS-iCre Tg/+ ; ROSA-stop-tTA KI/+
x
ROSA-stop-tTA KI/KI
ROSA-stop-tTA KI/KI
x
tetO-lines Tg/+ ; ROSA-stop-tTA KI/+
ROSA-stop-tTA KI/+
ROSA-stop-tTA KI/+
ROSA-stop-tTA KI/KI
NMS-iCre Tg/+ ; ROSA-stop-tTA KI/+
NMS-iCre Tg/+ ; ROSA-stop-tTA KI/KI
x
tetO-lines Tg/+ ; ROSA-stop-tTA KI/KI
tetO-lines Tg/+ ; ROSA-stop-tTA KI/+
ROSA-stop-tTA KI/KI
ROSA-stop-tTA KI/+
ROSA-stop-tTA KI/KI
NMS-iCre Tg/+ ; ROSA-stop-tTA KI/KI
tetO-lines Tg/+ ; ROSA-stop-tTA KI/KI
NMS-iCre Tg/+;tetO-lines Tg/+ ; ROSA-stop-tTA KI/KI
B
ROSA-stop-tTA KI/KI
x
PER2 LUC/LUC
ROSA-stop-tTA KI/+ ;PER2 LUC/+
x
ROSA-stop-tTA KI/+ ;PER2 LUC/+
ROSA-stop-tTA +/+ PER2 +/+
ROSA-stop-tTA +/+ PER2 LUC/+
ROSA-stop-tTA +/+ ;PER2 LUC/LUC
ROSA-stop-tTA KI/+ ;PER2 +/+
ROSA-stop-tTA KI/KI ;PER2 +/+
ROSA-stop-tTA KI/+ ;PER2 LUC/+
ROSA-stop-tTA KI/+ ;PER2 LUC/LUC
ROSA-stop-tTA KI/KI ;PER2 LUC/+
ROSA-stop-tTA KI/KI ;PER2 LUC/LUC
x
NMS-iCre Tg/+;tetO-lines Tg/+ ; ROSA-stop-tTA KI/KI
ROSA-stop-tTA KI/KI ;PER2 LUC/+
NMS-iCre Tg/+ ; ROSA-stop-tTA KI/KI ;PER2 LUC/+
tetO-lines Tg/+ ; ROSA-stop-tTA KI/KI ;PER2 LUC/+
NMS-iCre Tg/+;tetO-lines Tg/+ ; ROSA-stop-tTA KI/KI ;PER2 LUC/+

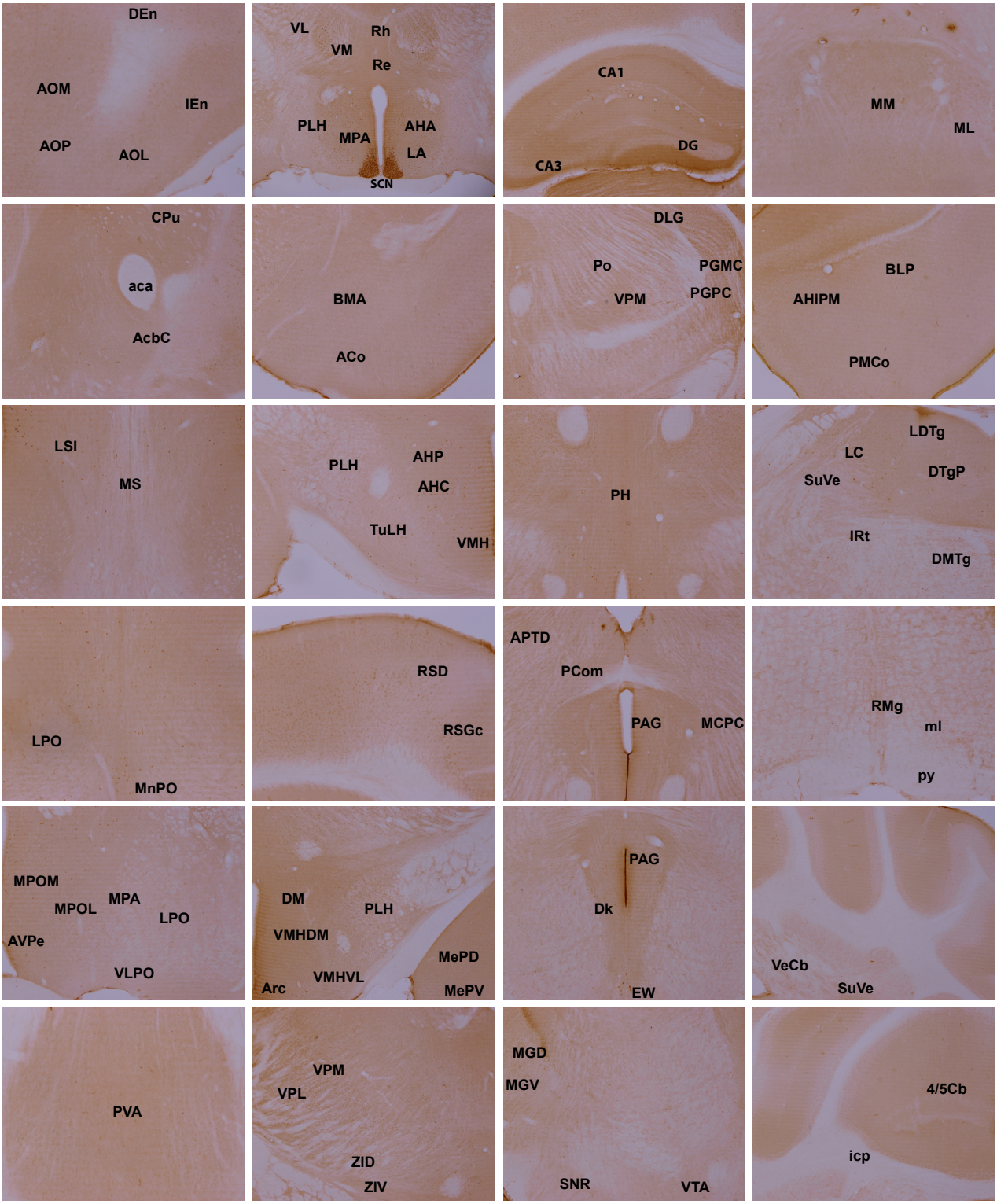
DEn
AOM
IEn
AOP
AOL
VL
Rh
VM
Re
PLH
MPA
AHA
LA
SCN
CA1
DG
CA3
MM
ML
CPu
aca
AcbC
BMA
ACo
DLG
Po
PGMC
VPM
PGPC
BLP
AHiPM
PMCo
LSI
MS
PLH
AHP
AHC
TuLH
VMH
PH
LDTg
LC
SuVe
DTgP
IRt
DMTg
LPO
MnPO
RSD
RSGc
APTD
PCom
PAG
MCPC
RMg
ml
py
MPOM
MPOL
MPA
LPO
AVPe
VLPO
DM
PLH
VMHDM
MePD
Arc
VMHVL
MePV
PAG
Dk
EW
VeCb
SuVe
PVA
VPM
VPL
ZID
ZIV
MGD
MGV
SNR
VTA
4/5Cb
icp

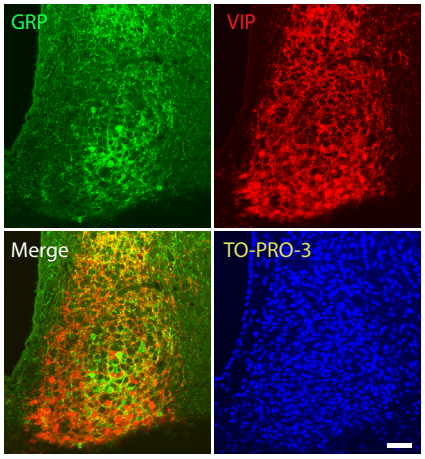

$\frac{\text{GRP+}}{\text{VIP+}}$ %	$\frac{\text{VIP+}}{\text{GRP+}}$ %
6.7±1.9%	21.7±1.2%

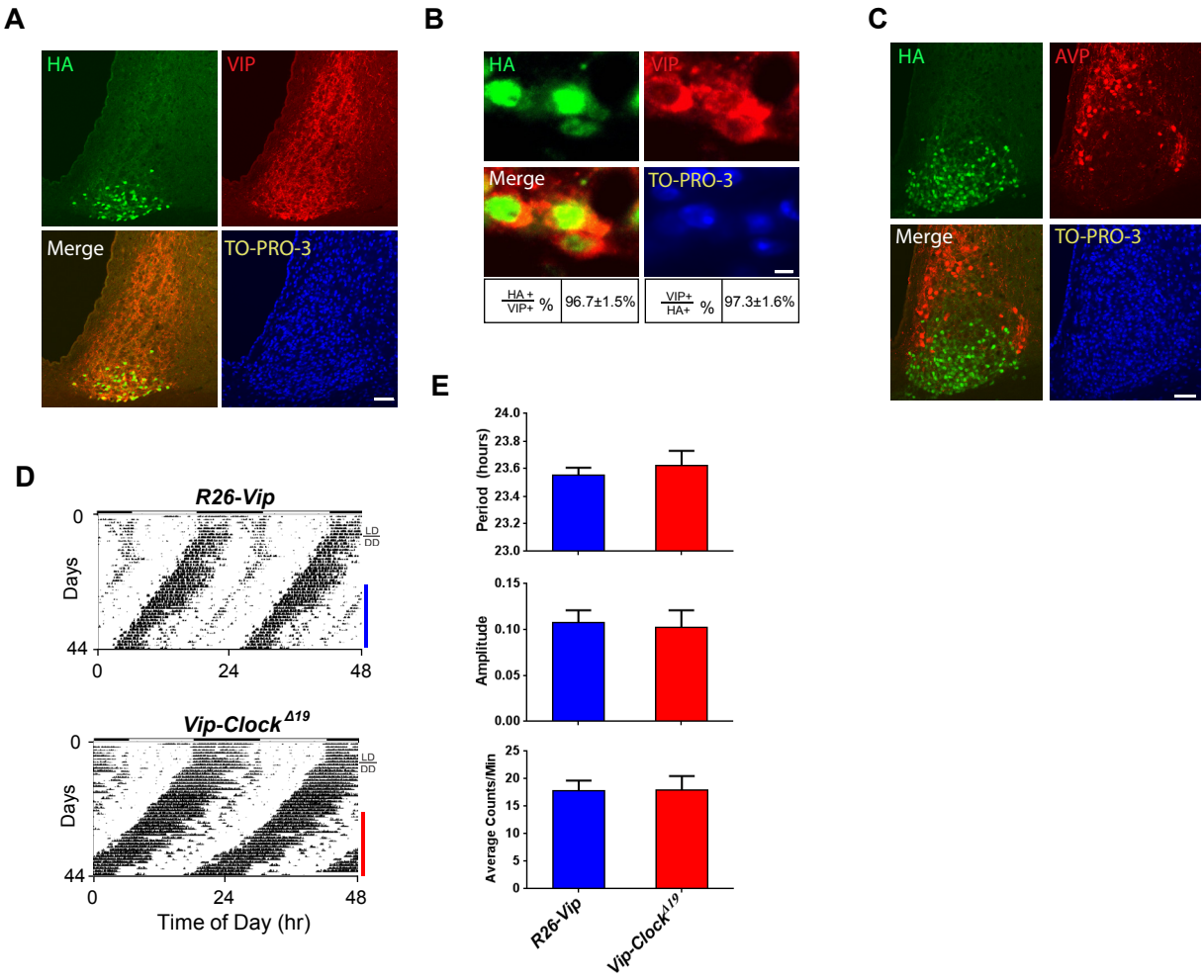
A
HA
VIP
Merge
TO-PRO-3
B
HA
VIP
Merge
TO-PRO-3
HA+/VIP+ %
96.7±1.5%
VIP+/HA+ %
97.3±1.6%
C
HA
AVP
Merge
TO-PRO-3
D
R26-Vip
Days
LD
DD
0
44
0
24
48
Vip-Clock Δ19
Time of Day (hr)
E
Period (hours)
24.0
23.8
23.6
23.4
23.2
23.0
Amplitude
0.15
0.10
0.05
0.00
Average Counts/Min
25
20
15
10
5
0
R26-Vip
Vip-Clock Δ19

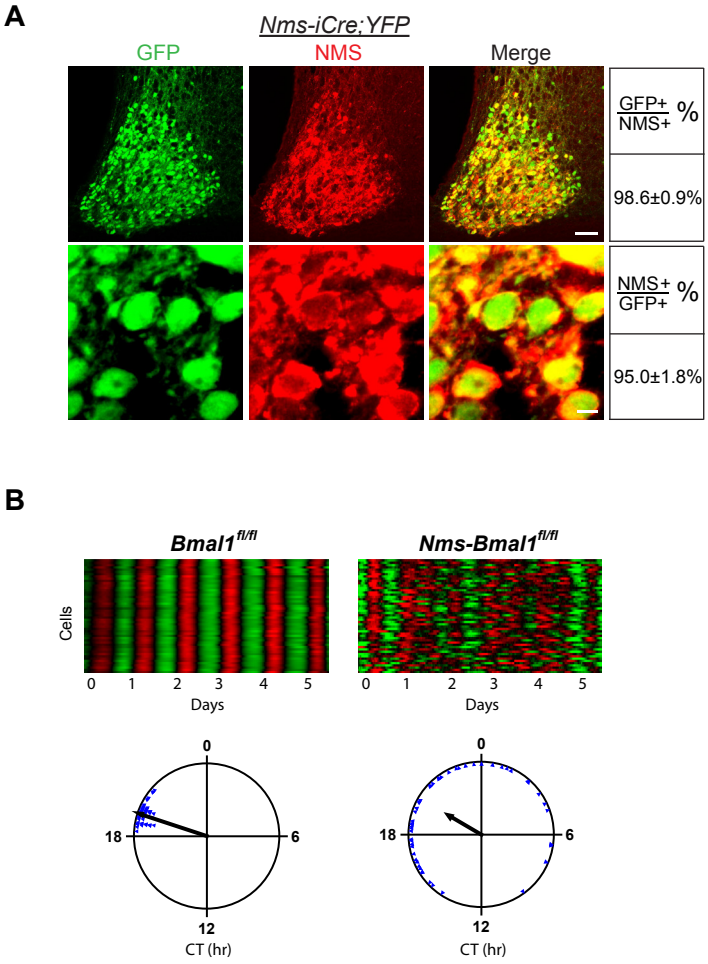
A
Nms-iCre;YFP
GFP
NMS
Merge
GFP+ / NMS+ %
98.6±0.9%
NMS+ / GFP+ %
95.0±1.8%
B
Bmal1fl/fl
Nms-Bmal1fl/fl
Cells
0 1 2 3 4 5
Days
0 1 2 3 4 5
Days
0
6
12
18
CT (hr)
0
6
12
18
CT (hr)

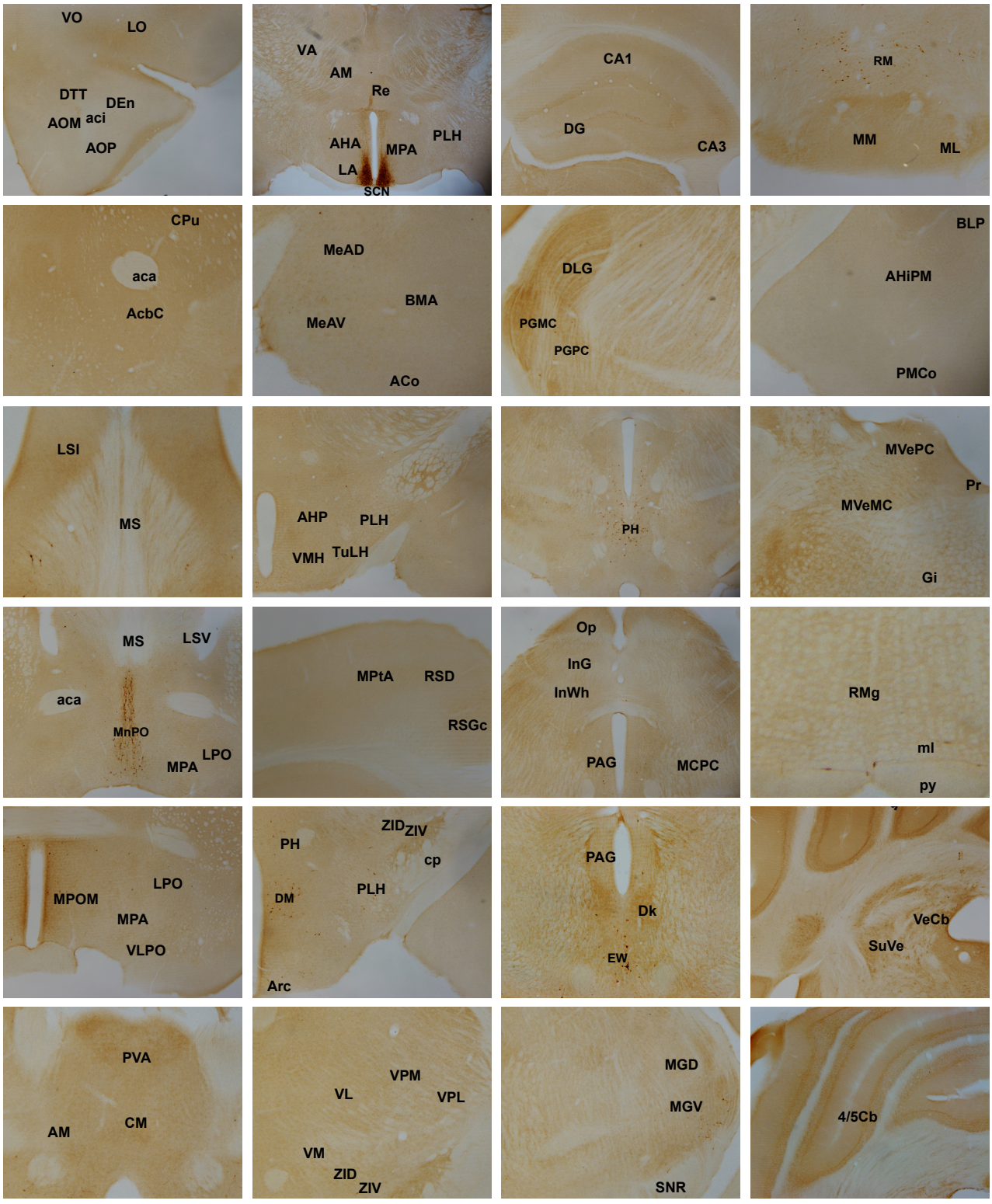
VO
LO
DTT
DEn
AOM
aci
AOP
VA
AM
Re
AHA
MPA
PLH
LA
SCN
CA1
DG
CA3
RM
MM
ML
CPu
aca
AcbC
MeAD
BMA
MeAV
ACo
DLG
PGMC
PGPC
BLP
AHiPM
PMCo
LSI
MS
AHP
PLH
VMH
TuLH
PH
MVePC
Pr
MVeMC
Gi
MS
LSV
aca
MnPO
MPA
LPO
MPtA
RSD
RSGc
Op
InG
InWh
PAG
MCPC
RMg
ml
py
LPO
MPOM
MPA
VLPO
ZID
ZIV
PH
cp
PLH
DM
Arc
PAG
Dk
EW
VeCb
SuVe
PVA
AM
CM
VPM
VL
VPL
VM
ZID
ZIV
MGD
MGV
SNR
4/5Cb

SUPPLEMENTAL EXPERIMENTAL PROCEDURES

Generation and Genotyping of *Nms-iCre* BAC transgenic and *Nms*$^{-/-}$ mice

A BAC construct that contains an IRES2-iCre cassette inserted into the 3'-UTR region of the *Nms* genomic sequence was generated by recombineering using BAC clone RP23-101P2 (CHORI BACPAC) and a plasmid containing an IRES2-iCre bicistronic expression cassette. The isolated *Nms-iCre* BAC DNA was injected into the pronucleus of C57BL/6N oocyte. Transmission of *Nms-iCre* was assessed by Taqman® probe real-time PCR assay using the following primer/probe sets:

5'- TGAGGGACTACCTCCTGTACC-3'

5'- ACACAGCATTGGAGTCAGAAG-3'

FAM-5'-AGCTCAACATGCTGCACAGGAGATCT-3'

The targeting vector used to generate *Nms*$^{-/-}$ contains a FRT flanked PGK-NEO cassette, a DTA cassette, and a Cre recombinase cassette from pBS185 (Gibco BRL) that replaces the start codon of *Nms* on exon 1 and deletes a 59 bp signal peptide sequence at the ATG start codon. The Cre cassette was not functionally utilized in experiments described here. A total of 480 neomycin resistant clones were screened by PCR which resulted in 9 positive clones. Upon confirmation with Southern blot analysis, three independent clones were microinjected into 129/SvEvTac blastocyst. After successful germ-line transmission, the Neo cassette was removed by crossing to a ROSA26-FLPe line. Transmission of *Nms*$^{-/-}$ was assessed by using 2 primer sets using a common forward primer:

Forward 5'-ACCCTCGGGAAATGCTCATCACCT-3'

Reverse null allele 5'-TCACTTGGTCGTGGCAGCCC-3'

Reverse WT allele 5'-GCCCATCACCTTTCAGTTTGGGGG-3'

All mice were backcrossed to C57BL/6J strain for at least five generations. All microinjections were performed by the UT Southwestern Transgenic Core facility.

Mouse breeding

To generate experimental mice efficiently, hemizygous *Nms-iCre* mice were crossed with *ROSA-STOP-tTA* mice for two generations to generate mice that are hemizygous for *Nms-iCre* and homozygous for *ROSA-STOP-tTA* (referred to as *R26-Nms*). Likewise, the hemizygous *tetO* lines (*tetO-Clock*$^{\Delta 19}$, *tetO-Per2*, and *tetO-TeNT*) were also bred individually with *ROSA-STOP-tTA* for two generations to generate mice that were hemizygous for the *tetO* transgene and homozygous for *ROSA-STOP-tTA* (referred to as *R26-Clock*$^{\Delta 19}$, *R26-Per2*, and *R26-TeNT*, respectively). Subsequently, *R26-Nms* mice were crossed with *R26-Clock*$^{\Delta 19}$, *R26-Per2*, or *R26-TeNT* to generate mice that express the *tetO-Clock*$^{\Delta 19}$, *tetO-Per2*, and *tetO-TeNT* transgene, respectively, under the regulation of *ROSA-STOP-tTA* in *Nms*-expressing cells. These quadruple transgenic mice are referred to as *Nms-Clock*$^{\Delta 19}$, *Nms-Per2*, and *Nms-TeNT*. Littermate controls that lack either the *Nms-iCre* and/or the *tetO-* transgene are also produced from these crosses. For bioluminescence experiments, PER2::LUC mice (Yoo et al., 2004) were crossed with *ROSA-STOP-tTA* for at least two generations to produce mice homozygous for both alleles. Subsequently, these mice were crossed with *Nms-Clock*$^{\Delta 19}$, *Nms-Per2*, or *Nms-TeNT* to generate mice that carried a hemizygous copy of *Nms-iCre*, a homozygous copy of *ROSA-STOP-tTA*, a heterozygous copy of PER2::LUC, and a hemizygous copy of *tetO-Clock*$^{\Delta 19}$, *tetO-Per2*, or *tetO-TeNT*, respectively. *Nms-TeNT;SynGFP* mice were generated in a similar manner by crossing *Nms-TeNT* mice to *tetO-SynGFP* mice with homozygous copies of *ROSA-STOP-tTA.* To generate *Vip-Clock*$^{\Delta 19}$ mice which contain a hemizygous copy of *tetO-Clock*$^{\Delta 19}$ and homozygous

copies of *Vip-Cre* and *ROSA-STOP-tTA*, *Vip-Cre* mice (Taniguchi et al., 2011) and *R26-Clock*$^{\Delta 19}$ mice (described above) were used in multiple sequential crosses which also resulted in the production of *R26-Vip* mice for experimental control. *Nms-Bmal1*$^{fl/fl}$ was generated by crossing *Nms-iCre* mice to *Bmal1*$^{fl/fl}$ mice (Storch et al., 2007) for at least two generations. *Nms-Bmal1*$^{fl/fl}$*;Luc* was generated by crossing *Nms-Bmal1*$^{fl/fl}$ to PER2::LUC for several generations. *Nms-iCre;YFP* and *Nms-Bmal1*$^{fl/fl}$*;YFP* mice were generated by crossing *Nms-iCre* or *Nms-Bmal1*$^{fl/fl}$ to ROSA-STOP-YFP mice (Srinivas et al., 2001) for at least two generations, respectively, to generate mice that have homozygous copies of ROSA-YFP along with *Nms-iCre* or *Nms-Bmal1*$^{fl/fl}$. *Nms*$^{-/-}$*Nmu*$^{-/-}$ mice were generated by crossing *Nms*$^{-/-}$ to *Nmu*$^{-/-}$ mice (Hanada et al., 2004) for at least two generations to generate double homozygous *Nms*$^{-/-}$*Nmu*$^{-/-}$ mice along with WT, *Nms*$^{-/-}$, and *Nmu*$^{-/-}$ mice. All experimental mice used were backcrossed to C57BL/6J for at least 5 generations.

Doxycycline (Dox) treatment

Doxycycline hyclate (Sigma-Aldrich; D9891) was given *ad libitum* in drinking water at a concentration of 10 μg/ml for all mice as described except for *Nms-TeNT* mice and related controls which were given 20 μg/ml of Dox. All Dox were renewed every 3 to 4 days (Hong et al., 2007). All mice were given free access to regular food.

Immunohistochemistry (IHC) and In Situ Hybridization (ISH)

IHC and ISH experiments were performed similarly as described previously (Chemelli et al., 1999)**.** Mice were anesthetized with ketamine/xylazine/saline cocktail (ketamine, 10 mg/ml; xylazine, 2 mg/ml) at 0.01 ml/g and intracardially perfused with 5-10 ml of 0.9% saline solution followed by 50 ml of 4% paraformaldehyde (Sigma-Aldrich) in PBS, pH 7.4. Brains were removed and postfixed overnight at 4°C in 4% paraformaldehyde. Coronal sections (50 μm

thick) were prepared using a Vibratome (Leica Microsystems). Free-floating sections were blocked in 3% normal goat serum (Vector Laboratories) with phosphate-buffered saline (PBS; pH 7.4) containing 0.3% Triton X-100 at room temperature for 1 h, followed by incubation with primary antibodies in PBS + 3% normal goat serum and 0.3% Triton X-100. After 2 overnight incubation of primary antibodies in 4°C, sections were washed 3 times with PBS and stained with the appropriate secondary antibodies in PBS + 0.3% Triton X-100 at room temperature for 1 h. Following this, sections were washed 3 times with PBS and incubated with TO-PRO-3 1:100 (Invitrogen) at room temperature for 1 h. For stereological counting, sections were incubated with NeuroTrace® 530 Red Fluorescent Nissl Stain 1:100 (Invitrogen). After staining, all sections were washed and mounted with ProLong® Gold Antifade Reagent with DAPI (Invitrogen). Primary antibodies used were rat anti-HA 1:100 (Roche), rabbit anti-NMS 1:1000 (Bachem), rabbit anti-BMAL1 (Novus Biologicals), guinea pig anti-VIP 1:2000 (Phoenix Pharmaceuticals), rabbit anti-AVP 1:4000 (Immunostar), rabbit anti-GRP 1:500 (Immunostar), chicken anti-GFP 1:500 (Invitrogen), rabbit anti-GFP 1:500 (Invitrogen), rabbit anti-VAMP2 (Synaptic Systems), and guinea pig anti-PER2 1:2000 (Yoo et al., 2013). Secondary antibodies include goat anti-rat Alexa 488 1:500 (Invitrogen), goat anti-chicken Alexa 488 1:500 (Invitrogen), goat anti-rabbit Alexa 488 1:500 (Invitrogen), goat anti-rabbit Alexa 546 1:500 (Invitrogen), and goat anti-guinea pig Alexa 546 1:500 (Invitrogen). For detection of NMS, VIP, and GRP cell bodies, colchicine (10-20 μg) was stereotaxically infused into the lateral cerebral ventricles of experimental mice 24-48 h before fixation.

For in situ hybridization, a 415 bp cDNA fragment was subcloned into pBluescript II SK(+) vector. Antisense riboprobes were generated with T7 RNA polymerase using the Maxiscript kit (Ambion) in the presence of 35S-CTP and 35S-UTP (MP Bio). Forebrain regions

were dissected from three C57BL/6J mice. Every fourth 35 μM coronal section was processed and used for ISH.

IHC image collection and analyses

Fluorescence-immunolabeled images were acquired using a Zeiss LSM 510 confocal microscrope. Post-imaging processing and co-localization analyses were performed using ImageJ. In all co-localization studies, 2-3 mice were used for each pair of analysis. Cells from every other section were used, resulting in 8-10 SCN sections of 50 μM thickness for each individual mouse. Only cells showing levels of expression clearly above background were counted.

Stereological cell counting

Fluorescence staining was visualized and subjected to stereological analysis using an Olympus BX-51 microscope and Stereo Investigator software (MBF Bioscience). Every other coronal section (50 μm thick) spanning the entire SCN from one brain hemisphere was counted using the Optical Fractionator workflow. A grid size of 80 x 80 μm and a frame size of 25 x 25 μm were used for anti-HA stained slices. For NeuroTrace Nissl staining, a grid size of 60 x 60 μm and a frame size of 20 x 20 μm were used. All contours were drawn at low magnification (10X, 0.3 NA) and counted at high magnification (100X oil, 1.3 NA). In all samples, the coefficient of error (CE, Gundersen m=0), a measure of the precision of stereological estimates (Gundersen and Jensen, 1987), ranged from 0.08-0.11.

Explant culture and bioluminescence data analysis

All mice used for explants cultures were raised on water and were at least 8 weeks of age at the time of experimentation. Following methods described previously (Yamazaki and Takahashi, 2005; Yoo et al., 2004), after cervical dislocation, the brain was removed and placed immediately in Hank balanced salt solution (HBSS; with 10 mM HEPES, 25 units/ml penicillin,

and 25 μg/ml streptomycin) on ice. Coronal slices containing the SCN were sectioned at 300 μm using a vibratome, followed by manual dissection of the SCN, resulting in a tissue approximately 1 mm by 1 mm in size. Dissected SCN tissues were cultured on a Millicell culture membrane (PICMORG50, Millipore) with 1.2 ml DMEM medium (Cellgro), supplemented with 10 mM HEPES (pH 7.2), 2% B27 (Invitrogen), 25 units/ml penicillin, 25 mg/ml streptomycin, and 0.1 mM luciferin (Promega). Explant cultures were maintained at 36°C in an incubator or in a temperature-controlled room. Bioluminescence was continuously monitored without interruption for >7 d immediately upon placement in culture using LumiCycle 32 luminometers (Actimetrics, Wilmette, IL).

For bioluminescence analyses, LumiCycle software (Actimetrics) was used to subtract the 24 hour moving average from the raw luminescence data and smoothed by 0.5 h adjacent averaging (Pendergast et al., 2009). To determine the period, baseline-subtracted and smoothed data were exported to ClockLab (Actimetrics) and determined by fitting a regression line to the acrophase of at least 3 days of the PER2::LUC rhythm. To quantitatively assess amplitude, the third stable peak of the baseline-subtracted, smooth data was assessed. All values are displayed as the mean ± SEM.

Single-cell bioluminescence imaging and data analysis

SCN explants were sectioned and cultured as described above. All mice used were raised on water. Bioluminescence recording was performed in a similar manner as previously described (Buhr et al., 2010; Welsh et al., 2004) with some modifications. Cultures containing individual SCN explants were placed on an inverted microscope (Leica DMIR) mounted on an anti-vibration table (TMC) placed within a heated Lucite chamber (Solent Scientific, UK) maintained at 37ºC. The stage, attached with a temperature sensor, was maintained at 37 ± 0.1ºC throughout

the experiment. During image acquisition, the entire setup was enclosed in a light-tight cabinet with inlets and outlets for cables and cryo-tubes.

Imaging recording was performed using a cryo-cooled 600 Series CCD camera (Spectral Instruments, Tucson, AZ) equipped with a 20X, 0.3 NA objective, and the camera was operated at -100ºC and 4 x 4 binning of a 2048 x 2048 pixel array during image acquisition. Each exposure/readout cycle was 15 min, and 32 bit images were collected and stored. Image stacks were then analyzed using ImageJ (NIH). Cosmic ray signals were removed using a top-hat filter with a radius of 2-pixels and threshold of 50. Kalman filter was then applied for smoothing. Subsequently, the bioluminescence values of each cell in the image sequence were outlined individually within a region of interest (ROI) and exported into Excel (Microsoft, Redmond, WA), where values were detrended by subtraction of baseline bioluminescence based on a running average from 12 hrs before to 12 hrs after each time point. The baseline-subtracted data was curve fitted to a modified damped sine wave in Prism (Graphpad) using the equation: Y= Amplitude*exp(-K*X)*sin((2*π*X/Wavelength)-Phase*2*π/Wavelength), wherein K is the damping constant, and the wavelength, phase, and amplitude were determined by the best-fit results. Heat-maps of Z-score normalized data were arranged by phase calculated from the above formula and plotted using the program MeV. Circadian phase clustering was assessed by Rayleigh's test and plotted with Oriana software (Kovach Computing Services, Anglesey, UK).

SUPPLEMENTAL REFERENCES

Buhr, E.D., Yoo, S.H., and Takahashi, J.S. (2010). Temperature as a universal resetting cue for mammalian circadian oscillators. Science *330*, 379–385.

Chemelli, R.M., Willie, J.T., Sinton, C.M., Elmquist, J.K., Scammell, T., Lee, C., Richardson, J.A., Williams, S.C., Xiong, Y., Kisanuki, Y., et al. (1999). Narcolepsy in orexin knockout mice: molecular genetics of sleep regulation. Cell *98*, 437–451.

Franklin, B.J., and Paxinos, G.T. (2008). The Mouse Brain in Stereotaxic Coordinates (New York, Academic Press).

Welsh, D.K., Yoo, S., Liu, A.C., Takahashi, J.S., and Kay, S.A. (2004). Bioluminescence imaging of individual fibroblasts reveals persistent, independently phased circadian rhythms of clock gene expression. Curr Biol. *14*, 2289–2295.

Yoo, S.H., Mohawk, J.A., Siepka, S.M., Shan, Y., Huh, S.K., Hong, H.-K., Kornblum, I., Kumar, V., Koike, N., Xu, M., et al. (2013). Competing E3 Ubiquitin Ligases Govern Circadian Periodicity by Degradation of CRY in Nucleus and Cytoplasm. Cell *152*, 1091–1105.